Simplifications of the bilinear transfer for microscopic binary objects

D. Courjon, D. Charraut, Georges Boudebs

Simplifications of the bilinear transfer for microscopic binary objects

D. Courjon, D. Charraut, and G. Bou Debs

Laboratoire d'Optique P. M. Duffieux, Centre National de la Recherche Scientifique, Unité Associée 214, Faculté des Sciences et des Techniques, Université de Franche-Comté-Besançon, 25030 Besançon Cedex, France

Microscopy of binary objects in partially coherent light is analyzed in terms of bilinear transfer. A transfer model using two apparent transfer functions is proposed. Its domain of validity is studied by numerical simulation.

1. INTRODUCTION

The deduction of features of scattering objects from the measurement of the emitted and scattered fields is an optical problem, the importance of which is growing in numerous fields such as metrology and biology.[1] Experimentally, various methods can be used: for instance, the direct analysis of the light field propagating in free space or the use of optical processors as imaging systems. In the latter case, optical microscopy in partially coherent light is still attractive, since it involves a simple instrument that is easy to use and that remains efficient for objects whose dimensions are of several wavelengths.[2] Moreover, owing to partial coherence, a scalar approach of the transfer is generally sufficient for describing the image formation accurately. Unfortunately, the partial coherent transfer is inherently nonlinear, and it is generally not possible, without restrictive hypotheses or prior knowledge, to determine the object distribution from its magnified image. In order to determine with accuracy the parameters of a given object, it is necessary to define, first, a unique relation between object and image distributions. The function connecting the object and image data is the bilinear transfer function (BTF) (also called the cross-coefficient function) in partially coherent light.[3,4] Although the notion of bilinear transfer has simplified the mathematical formalism of the partially coherent imagery, its utility is not obvious in practice.

The first approach to solving the inverse problem is to use a numerical procedure, which is today possible by means of the current numerical capacities. However, this approach presents some drawbacks involving the computing time, which cannot be neglected in certain cases requiring real-time dimensional control, involving signal processing; moreover, a numerical approach requires a precise knowledge of the different parameters defining the system.

Several authors have tried to simplify the transfer by introducing the notion of an apparent transfer function (ATF),[5] which depends on the class of objects that are considered (nature, shape, size, etc.). Despite this restriction, such a function simply connects object and image spectra and thus permits the retrieval of the object features from the image irradiance.

A practical example of transfer modeling was recently developed in a study of linewidth measurement technology.[6] In that study, a simplified form of the partially coherent transfer equation was found experimentally. The simplification, which is based on the decomposition of the overall transfer into two partial ones, permits the use of a fast numerical method for accurately retrieving the linewidth from the image spectrum data.

This paper is intended to complete these experimental works with a theoretical approach by analyzing the transfer in partially coherent light for rectangular objects. It is shown that the modeling is well adapted for explaining the image behavior and, for example, the overshots that appear at the transition regions in the object.

Finally, the modeling is tested by means of numerical simulations, and the role of each partial transfer on the image and its Fourier spectrum is pointed out.

2. THEORY

Let us consider the space-invariant and inversion-invariant imaging system described in Fig. 1. The different optical elements are the thermal source S_0, the field condenser lens L_0, the condenser C, the object O, and the objective Ob.

A. Transfer Relation

The system can be described by the well-known transfer integral[7]

$$\tilde{I}\left(\frac{\mathbf{u}}{\lambda p'}\right) = \iint \mathcal{T}(\mathbf{u}+\mathbf{u}', \mathbf{u}')\tilde{O}\left(\frac{\mathbf{u}+\mathbf{u}'}{\lambda p}\right)\tilde{O}^*\left(\frac{\mathbf{u}'}{\lambda p}\right)\mathrm{d}^2u'. \quad (1)$$

$\mathbf{u}$ and $\mathbf{u}'$ are the position vectors $\mathbf{u}(u_1, u_2)$ and $\mathbf{u}'(u_1', u_2')$ in the frequency plane, $\tilde{I}$ is the Fourier transform of the image irradiance, $\tilde{O}$ is the Fourier transform of the object transmittance (or reflectance), $\mathcal{T}$ is the BTF, λ is the wavelength, and p and p' are the distances from the object plane to the entrance pupil plane and from the exit pupil plane to the image plane, respectively. By putting

$$\boldsymbol{\omega} = \mathbf{u}/\lambda p, \qquad \boldsymbol{\omega}' = \mathbf{u}'/\lambda p, \qquad p'/p = g$$

and introducing the new functions

$$T(\boldsymbol{\omega}, \boldsymbol{\omega}') \equiv \mathcal{T}(\boldsymbol{\omega} \cdot \lambda p, \boldsymbol{\omega}' \cdot \lambda p), \quad (2)$$

$$\tilde{I}(\boldsymbol{\omega}) \equiv \tilde{I}(\boldsymbol{\omega}/g), \quad (3)$$

Eq. (1) can be then rewritten as

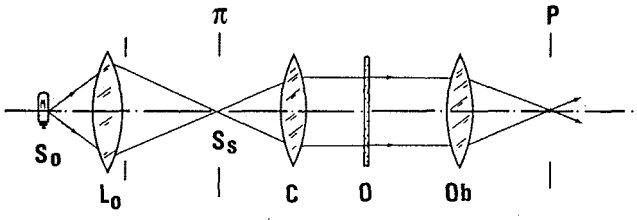

Fig. 1. Microscope in Köhler's illumination. The image S_S of the thermal source (S_0) is projected in the pupil plane (P) of the objective (Ob).

$$\tilde{I}(\omega) = \iint T(\omega + \omega', \omega')\tilde{O}(\omega + \omega')\tilde{O}^*(\omega')\mathrm{d}^2\omega', \tag{4}$$

where T takes the form

$$T(\omega, \omega') = \iint S(\alpha)P(\omega + \alpha)P^*(\omega' + \alpha)\mathrm{d}^2\alpha. \tag{5}$$

S is the emittance in the image of the source projected in the pupil plane, and P is the pupil transmittance.

The type of object under test belongs to the category of two-dimensional objects (flat ones) and is represented physically in Fig. 2. I_S and ϕ_S (I_M and ϕ_M) are the intensity and the phase of a plane wave Σ_S (Σ_M) after reflection on the object. The latter can then be described mathematically by the one-dimensional functions

$$\begin{aligned} O(x) &= O_R(x) + jO_J(x), \\ O_R(x) &= 1 - (1 - t_0 \cos\phi_0)\mathrm{rect}(x/L), \\ O_J(x) &= t_0 \sin\phi_0 \,\mathrm{rect}(x/L), \end{aligned} \tag{6}$$

where x is one of the coordinates of the position vector $\mathbf{r}(x, y)$ in the object plane, ϕ_0 is the phase difference $\phi_M - \phi_S$, and t_0 is the quantity $(I_M/I_S)^{1/2}$.

It was shown previously[8] that the two-dimensional integral in the right-hand side of Eq. (4) reduces to a one-dimensional one in the case of objects whose transmittance is constant along the y direction:

$$\tilde{I}(\omega) = \int T(\omega + \omega', \omega')\tilde{O}(\omega + \omega')\tilde{O}^*(\omega')\mathrm{d}\omega'. \tag{7}$$

$\tilde{I}(\omega)$ can be rewritten as a linear combination of two terms[6]:

$$\tilde{I}(\omega) = A\tilde{I}'(\omega) - 2B\tilde{I}''(\omega) \qquad \text{for } \omega \neq 0. \tag{8}$$

The term $\tilde{I}(0)$, which corresponds to a constant irradiance in the object, has been omitted for the sake of clarity:

$$\tilde{I}'(\omega) = \frac{1}{\pi^2}\int T(\omega + \omega', \omega')\frac{\sin[\pi(\omega + \omega')L]}{(\omega + \omega')} \times \frac{\sin(\pi\omega' L)}{\omega'}\mathrm{d}\omega' \tag{9}$$

and

$$\tilde{I}''(\omega) = \frac{1}{\pi} T(\omega, 0)\frac{\sin(\pi\omega L)}{\omega}. \tag{10}$$

Parameters A and B, which depend on only the object parameters, are defined as follows:

$$\begin{aligned} A &= 1 + t_0^2 - 2t_0 \cos\phi_0, \\ B &= 1 - t_0 \cos\phi_0. \end{aligned}$$

In order to continue the transfer modeling, it is necessary to simplify the integral term $\tilde{I}'(\omega)$, for instance, by developing $\sin[\pi(\omega + \omega')L]$ in sine and cosine functions and using the fractional expansion

$$\frac{1}{\omega'(\omega + \omega')} = \frac{1}{\omega}\left(\frac{1}{\omega'} - \frac{1}{\omega + \omega'}\right). \tag{11}$$

The Fourier transform of the image irradiance can then be rewritten in terms of a combination of three simpler terms:

$$\tilde{I}'(\omega) = \mathrm{sinc}(\pi\omega L)\tilde{I}_1(\omega) - \cos(\pi\omega L)[\tilde{I}_2(\omega) + \tilde{I}_3(\omega)], \tag{12}$$

where

$$\tilde{I}_1(\omega) = 2L^2 \int T(\omega + \omega', \omega')\mathrm{sinc}(2\pi\omega' L)\mathrm{d}\omega', \tag{13}$$

$$\tilde{I}_2(\omega) = \frac{1}{\pi^2\omega}\int \frac{T(\omega + \omega', \omega')}{\omega'} \cos(2\pi\omega' L)\mathrm{d}\omega', \tag{14}$$

$$\tilde{I}_3(\omega) = -\frac{1}{2\pi^2}\int \frac{T(\omega + \omega', \omega')}{(\omega + \omega')\omega'}\mathrm{d}\omega'. \tag{15}$$

The sinc function is the ratio $\sin(\pi\omega L)/\pi\omega L$. $\tilde{I}_3(\omega)$ can be rewritten as

$$\tilde{I}_3(\omega) = -\frac{1}{\pi^2\omega}\int \frac{T(\omega + \omega', \omega')}{\omega'}\mathrm{d}\omega' \tag{16}$$

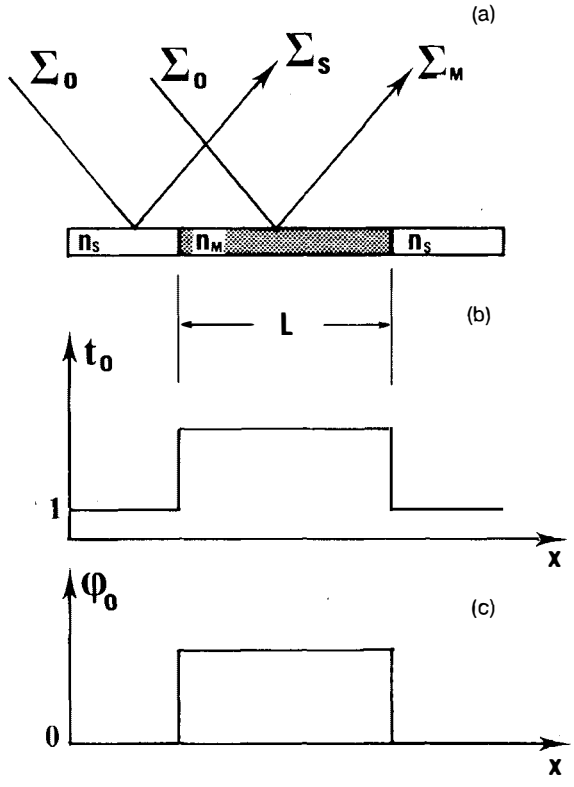

Fig. 2. (a) Schematic representation of the object; n_S and n_M are the indices of the two media constituting the object. Plane waves before (Σ_0) and after (Σ_S and Σ_M) reflection over the object are shown. (b), (c) Variation of T_0 and ϕ_0 over the object.

by using the symmetry properties of the BTF[4]:

$$T(\omega, \omega') = T^*(-\omega', -\omega),$$

which is due to the reality of the image irradiance, and

$$T(\omega, \omega') = T^*(\omega, \omega'),$$

which holds for inversion-invariant and space-invariant bilinear systems.

It is not possible to reduce the evaluation of the integrals further, except with approximations that are compatible with the experimental conditions. These approximations are studied in the Subsection 2.B.

B. Approximated Solutions for Integrals $\tilde{I}_1$, $\tilde{I}_2$, and $\tilde{I}_3$

It is supposed that the coherent cutoff frequency is several times as large as the frequency of the first zero in the spectrum of rectangular objects. This assumption means simply that the microscope works under good conditions, i.e., sufficiently below the resolution limit.

With this hypothesis the integrals given in Subsection 2.A can be simplified.

Let us consider, first, the integral on the right-hand side of Eq. (13). It contains the product of the BTF $T(\omega, \omega')$ with a sinc function related to the object. With conventional optics and in partially coherent illumination, the BTF has the aspects represented in Figs. 3(a) and 3(b) for circular apertures and one-dimensional apertures, respectively. It exhibits a constant region and a decreasing part, the relation of which depends on the degree of coherence of the light.[4,7] Consequently, the BTF variations are generally small for conventional systems. Inversely, the sinc function is twice as narrow as the Fourier spectrum of a rectangle function of the same width as that of the object. It is thus much more narrow than the BTF extension. In this case the value of the integral is different from zero only in the vicinity of $\omega' = 0$, and Eq. (13) reduces to

$$\tilde{I}_1 \simeq LT(\omega, 0), \tag{17}$$

where $T(\omega, 0)$ is the value of the BTF along the axis $\omega' = 0$.

Let us consider now the integral in Eq. (14). In microscopy, the cutoff frequency of the imaging system is always many times larger than the frequency of the first zero of the function $\mathrm{sinc}(\pi\omega L)$ in order to form a well-resolved image in the output plane. The integrand on the right-hand side of Eq. (14) is thus the product of an extended slowly varying function, $T(\omega + \omega', \omega')$, and a rapidly oscillating term $\cos(2\pi\omega' L)/\omega'$. Consequently, the value of the integral is sufficiently small, in comparison with the previous one, to be neglected. We shall use numerical simulations to demonstrate more clearly the limits of the validity of these approximations.

The last term [Eq. (15)] is certainly the most interesting one, since the integral does not contain information about the object. It is generally not negligible, and it plays a key role in the transfer process, as is shown in Section 3.

Finally, for large objects, taking into account the values of $\tilde{I}_1$ and $\tilde{I}_3$, the image spectrum can be written as the difference of two terms,

$$\tilde{I}(\omega) \simeq L(A - 2B)\mathrm{sinc}(\pi\omega L)T_{A1} - A\cos(\pi\omega L)T_{A2}, \tag{18}$$

where

$$T_{A1} = T(\omega, 0) \tag{19}$$

is the first nonnormalized ATF and

$$T_{A2} = I_3 = -\frac{1}{\pi^2\omega}\int \frac{T(\omega + \omega', \omega')}{\omega'}\,\mathrm{d}\omega' \tag{20}$$

is the second nonnormalized ATF.

We note that in the domain of validity of our hypotheses, the two ATF's do not depend on the width of the object under test. The partially coherent transfer is thus equivalent to the juxtaposition of two transfers working in parallel. The first transfer, associated with the ATF T_{A1}, acts as an incoherent transfer, where the modulation transfer function would be replaced by $T(\omega, 0)$. The sinc function is merely the Fourier transform of the object emittance. The shape of the function $T(\omega, 0)$ can be deduced easily from the three-dimensional representation of the BTF in Fig. 3.

The second transfer is not so classical. The cosine function can be explained as the contribution of the object edges. In our precise case of a binary object it is the Fourier transform of the derivative of the object emittance. Its role is pointed out more clearly in the numerical simulation.

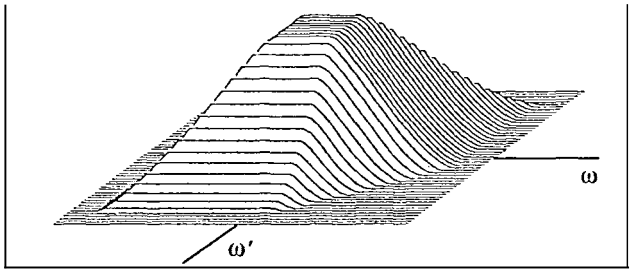

(a)

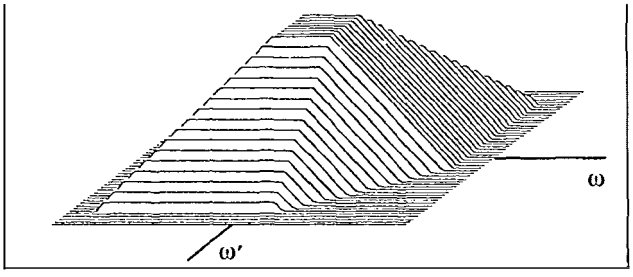

(b)

Fig. 3. Three-dimensional representation of the BTF in partially coherent light (a) for a circular objective aperture and (b) for a one-dimensional aperture (coherence coefficient, $\sigma = 0.67$).

3. NUMERICAL SIMULATION

In the development in Section 2, the only condition on the system is that $T(\omega, \omega')$ vary slowly related to ω or ω'. Our conclusions are thus valid for any classical imaging system. Let us now consider the practical case of partially coherent microscopy.

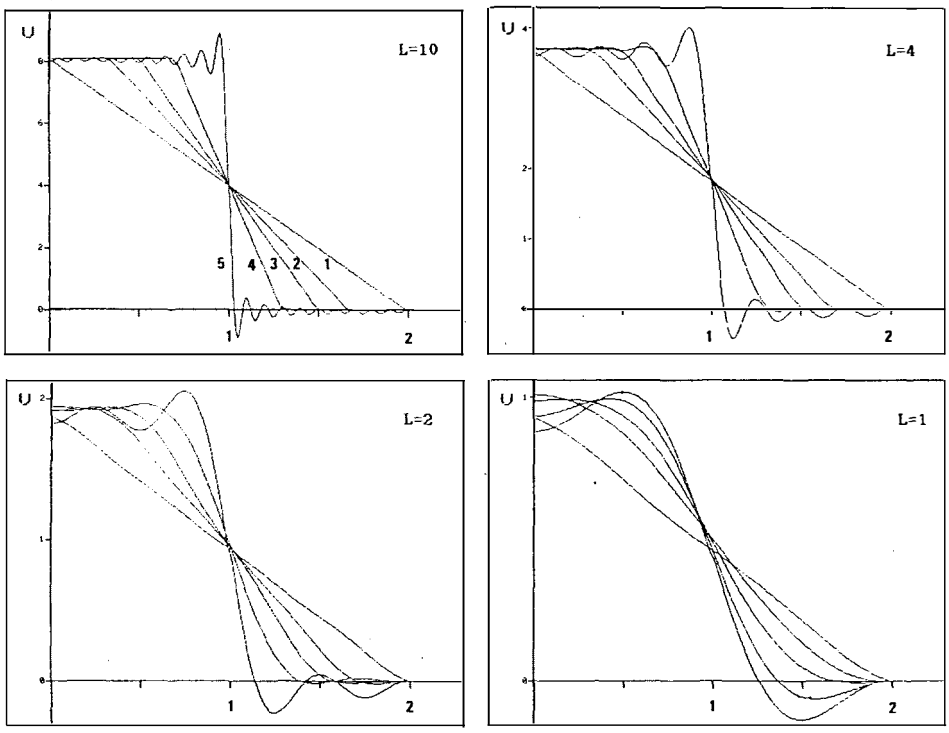

Fig. 4. Integral I_1 plotted for various coherence coefficients and various object widths. (U is in arbitrary units.) Curves 1, $\sigma = 1$; curves 2, $\sigma = 0.67$; curves 3, $\sigma = 0.50$; curves 4, $\sigma = 0.30$; curves 5, $\sigma = 0.01$.

It was shown recently[9] that, for uniform full sources and pupils, the BTF is modified slightly when the conventional two-dimensional functions are replaced in Eq. (5) by one-dimensional equivalent functions. This point is illustrated in Fig. 3. In this case

$$\begin{aligned} S(\alpha) &= 1 \quad \text{if } |\alpha| \leqslant r \\ &= 0 \quad \text{if } |\alpha| > r, \\ P(\alpha) &= 1 \quad \text{if } |\alpha| \leqslant R \\ &= 0 \quad \text{if } |\alpha| > R, \end{aligned}$$

where α is one of the coordinates of the position vector $\boldsymbol{\alpha}$.

Since the source and the pupil are now constant, it is possible to introduce the ratio

$$\sigma = r/R,$$

called the coherence coefficient. It is defined as the ratio of the radius of the image of the source projected in the exit pupil plane to the radius of the pupil aperture. Theoretically σ varies from 0 (coherent illumination) to infinity (incoherent illumination), but often the highest value of σ is about 1 (especially in reflection microscopy), corresponding to incoherent fields.

Integrals $\tilde{I}_1$, $\tilde{I}_2$, and $\tilde{I}_3$ are numerically calculated for various values of the coherence coefficient, $\sigma = 0.01, 0.3, 0.5, 0.67, 1$ ($\sigma = 0.67$ is a value often used in microscopy), and for various values of the object width, $L = 1, 2, 4, 10$, corresponding physically to actual lengths, $L_E = 0.54, 1.08, 2.16, 5.4$ μm, with a numerical aperture N.A. = 0.95 and $\lambda = 0.5145$ μm. The resulting curves are given in Figs. 4 and 5.

Note that it is obvious that the notion of large or small objects has no sense without a given reference, for instance, the coherent limit frequency of the system. The frequency ω_0 of the first zero in the object spectrum is given by $1/L$. For large objects [for example $L = 4$, $\omega_0 = 0.25$, which is 4 times as small as the coherent limit frequency ($\omega_c = 1$)], the resulting image can be resolved well theoretically, whereas for small objects (for example, $L = 1$, $\omega_0 = \omega_c = 1$), the image is strongly affected by the limited resolution of the system.

A. Discussion of the Curves

Integral $\tilde{I}_1$ [Eq. (13), Fig. 4]

Let us recall that we have assumed that

$$\tilde{I}_1 \simeq LT(\omega, 0)$$

in our working conditions.

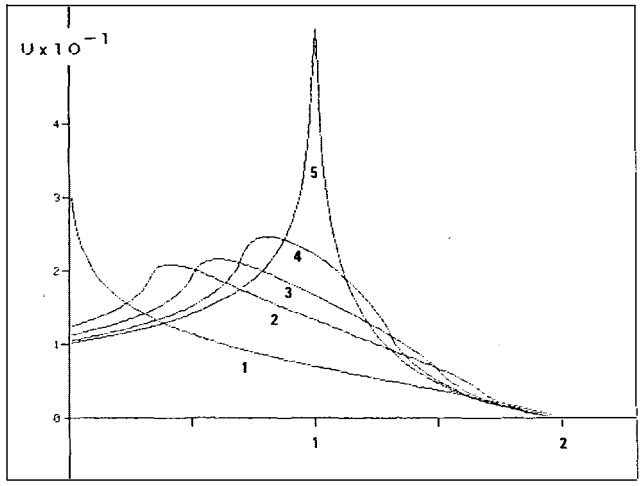

Fig. 5. Integral I_3 for the same coherence coefficients as in Fig. 4.

This approximation is justified effectively in a large range of metrological applications in partially coherent illumination even for submicrometer objects.

Integral $\tilde{I}_2$ [Eq. (14)]
The case of integral $\tilde{I}_2$ is not illustrated here. The integral can be neglected regardless of the coherence coefficient and the width of the object.

Integral $\tilde{I}_3$ [Eq. (16), Fig. 5]
The term on the right-hand side of Eq. (16) corresponds to the ATF T_{A2}. It does not depend on the object width L. The shape of the curve varies significantly when the coherence of the illumination beam changes. It is well known that the sharp transitions of the transfer functions are responsible for oscillations in the images. It is interesting here that $\sigma = 0.67$ corresponds to an ATF T_{A2} that varies slowly in the whole range of spatial frequencies.

B. Fourier Spectrum of the Image

It is now interesting to compare the spectrum of the image obtained directly from the transfer equation and that obtained after modeling. Let us then introduce the physical parameters

$$\begin{aligned} \lambda &= 0.5145\ \mu\text{m}, \\ \text{N.A.} &= 0.95, \\ \sigma &= 0.67, \\ L &= 2.5, \\ L_E &= 1.35\ \mu\text{m}, \\ \phi_0 &\simeq 85°, \\ t_0^2 &= 1.2, \end{aligned}$$

which are actual experiment conditions in linewidth measurement microscopy.

Figure 6 corresponds to the modulus of the image spectrum directly calculated from Eq. (7), i.e., without approximation (solid line) and after modeling (dotted line). We note the good similarity between the exact spectrum and the approximated one.

C. Image Reconstruction

To illustrate the effect of the simplifications on the image profile, the latter is reconstructed from the spectrum without approximation in Fig. 7(a) and from the approximated solution in Fig. 7(b). The validity of the modeling is confirmed even for small objects ($L = 2.5$, i.e., $L_E = 1.35\ \mu$m). This operation is performed by using a numerical inverse fast Fourier transform.

Moreover, it was predicted previously that the transfer depending on T_{A1} could be considered as describing the classical noncoherent transfer, the second term being connected to a derivative effect. This point is confirmed by the curves in Fig. 8, in which the contribution of each term of the spectrum is exhibited in the image plane.

It is clear from relation (18) that the relative weight of each elementary image depends on the object parameters t_0 and ϕ_0. For example, if

$$A - 2B = 0 \rightarrow t_0 = 1,$$

then the image is described only by Fig. 8(b). This result is well known; the image of a purely phase object exhibits variations of intensity only in the region of object transition. The proposed modeling permits us to associate with this phase-contrast effect a perfectly determined transfer function (T_{A2}) that can be calculated for any coherence degree.

It is also interesting that the transfer T_{A2} cannot be canceled for purely amplitude objects (i.e., $\phi_0 = 0$) because

$$A = (1 - t_0)^2 \neq 0 \quad \text{for} \quad t_0 \neq 1.$$

In other words, the overshots in the image are not due only

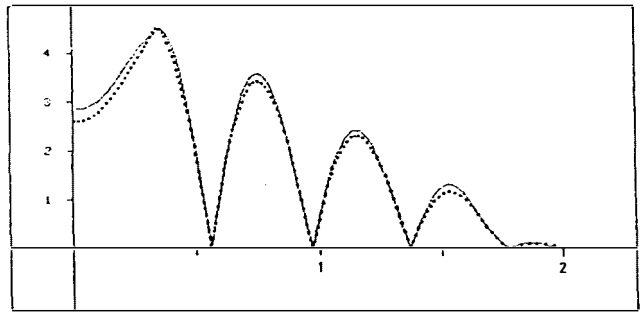

Fig. 6. Modulus of the image spectrum: solid line, plotted from Eq. (7), i.e., without approximation; dotted line, plotted after modeling. $L_E = 1.35\ \mu$m, $\lambda = 0.5145\ \mu$m, N.A. = 0.95, and $\sigma = 0.67$.

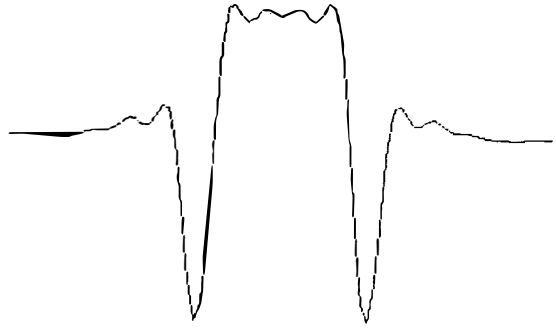

(a)

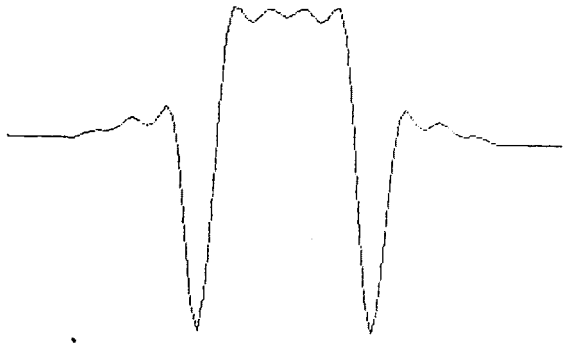

(b)

Fig. 7. Image profile obtained (a) without approximation (Fourier transform of the spectrum plotted in Fig. 6) and (b) after modeling.

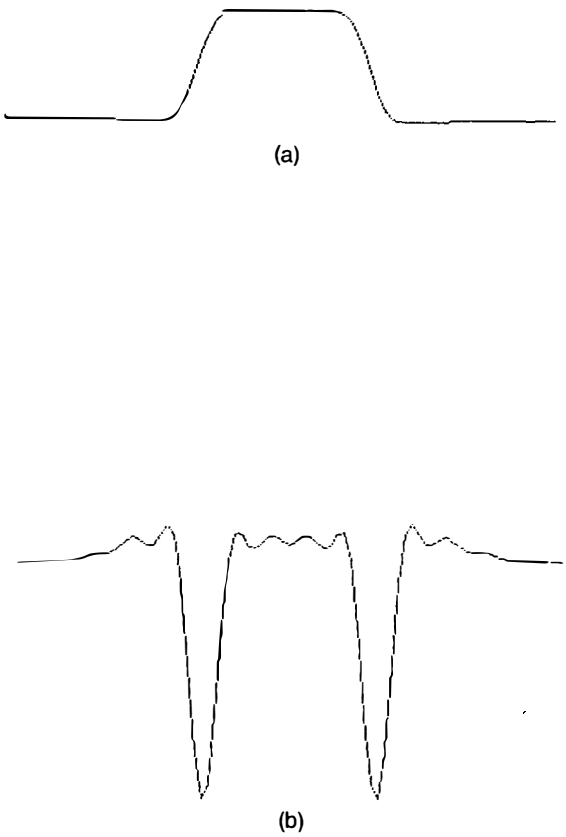

Fig. 8. (a) Partial image profile due to the first apparent transfer. (b) Partial image profile due to the second apparent transfer (derivative effect).

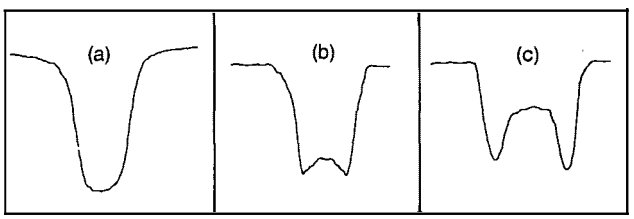

Fig. 9. Examples of experimental profiles for different parameters t_0 and ϕ_0: (a) $A - 2B > A$ (amplitude object $L_E \simeq 1.5\ \mu$m); (b) $A - 2B \simeq A$ (phase and amplitude object $L_E \simeq 1.5\ \mu$m); (c) $A - 2B < A$ (phase object $L_E = 2.5\ \mu$m). $\sigma = 0.67$, $\lambda = 0.5145\ \mu$m, N.A. = 0.95.

to the phase difference ϕ_0. To cancel the second transfer, it would be necessary to verify the equation

$$A = 1 + {t_0}^2 - 2t_0 \cos \phi_0 = 0;$$

that is,

$$\frac{(1 + {t_0}^2)}{2t_0} \leqslant 1,$$

which is never verified if $t_0 \neq 1$.

For reducing the overall transfer to only the first term, it is thus necessary to suppose low-contrast amplitude objects, that is,

$$t_0 = 1 \pm \epsilon, \qquad \phi_0 = 0.$$

In this case,

$$A \simeq 2t_0(1 - \cos \phi_0) = 0$$

and

$$A - 2B \simeq \pm 2\epsilon.$$

We again find the conditions of linearization of the bilinear transfer,[4] which can be met easily in practice.

All these cases are effectively encountered practically, as shown in Fig. 9.

D. Generalization of this Modeling

It is clear that perfectly rectangular objects are rarely met in practice even in integrated electronics. The usual sample object is one with slightly smoothed edges. Results of some experiments made on this type of object show that the proposed approach of the transfer remains valid.[6] It can be explained as follows: an object with smoothed edges can be described as a perfect rectangle in convolution with a smoothing function. The effect of the latter can be taken into account in the transfer, consequently introducing a small modification in the shapes of both T_{A1} and T_{A2}.

4. CONCLUSION

For rectangular two-dimensional objects (flat objects) the bilinear transfer can be simplified by introducing two particular ATF's. The first one acts on the Fourier spectrum of the intensity reemitted by the object. It thus has certain similarities with an incoherent transfer. The second ATF acts on a cosine function that is the Fourier transform of the object derivative. In the more general case of an object with slightly smoothed edges, it describes the edge transfer. Such a transfer modeling can be then considered a two-channel transmission, with the relative weight of each channel depending on the object parameters (ϕ_0 and t_0). The interest of such a modeling is, on the one hand, a simple interpretation of the image profile in partially coherent light and, on the other hand, the possibility of carrying out fast procedures to determine such critical parameters as the linewidth of wafers by solving relation (18) numerically. Images of microscopic objects of width from 0.8 μm to a few micrometers can be measured accurately.[6,10]

This modeling will be developed and extended in future studies to the more physical case of binary three-dimensional objects.

ACKNOWLEDGMENTS

This research was supported by the Centre d'Etudes des Télécommunications (CNET)-France (grant no. 85 3B 065 CNS). The authors thank M. Guillaume (CNET-Grenoble) and N. Noailly-Alcouffe (Société Microcontrôle) for providing a part of the numerical programs and also for useful discussions and criticisms.

REFERENCES

1. See, for example, H. P. Baltes, *Inverse Source Problems in Optics*, Vol. 9 of Topics in Current Physics, H. P. Baltes, ed. (Springer-Verlag, New York, 1978), pp. 119–154.
2. W. M. Bullis and D. Nyyssonen, "Optical linewidth measurements on photomasks and wafers," VLSI Electron. Microstructure Sci. **3**, 301–346 (1982).

3. H. H. Hopkins, "On the diffraction theory of optical images," Proc. R. Soc. London Ser. A **217,** 408–432 (1953).
4. B. Saleh, "Optical bilinear transformations: general properties," Opt. Acta **26,** 777–799 (1979).
5. R. Becherer and G. Parrent, "Nonlinearity in optical imaging systems," J. Opt. Soc. Am. **57,** 1479–1486 (1967).
6. M. E. Guillaume, N. Noailly, J. C. Reynaud, and J. L. Buevoz, "Fourier transform method for optical linewidth measurement," in *Integrated Circuit Metrology II*, D. Nyyssonen, ed., Proc. Soc. Photo-Opt. Instrum. Eng. **480,** 71–77 (1984).
7. M. Born and E. Wolf, *Principles of Optics* (Pergamon, Oxford, 1975), pp. 491–535.
8. E. Kintner, "Method for the calculation of partially coherent imagery," Appl. Opt. **17,** 2747–2753 (1978).
9. D. Courjon, D. Charraut, and P. Livrozet, "Bilinear transfer in microscopy," Opt. Acta **34,** 127–136 (1987).
10. M. E. Guillaume, N. Noailly, M. Pichot, and J. L. Buevoz, "Evaluation of a Fourier transform method for accurate critical dimension measurements," Microcircuit Eng. **3,** 211–218 (1985).